Figures and figure supplements

Structural basis of malodour precursor transport in the human axilla

Gurdeep S Minhas *et al*

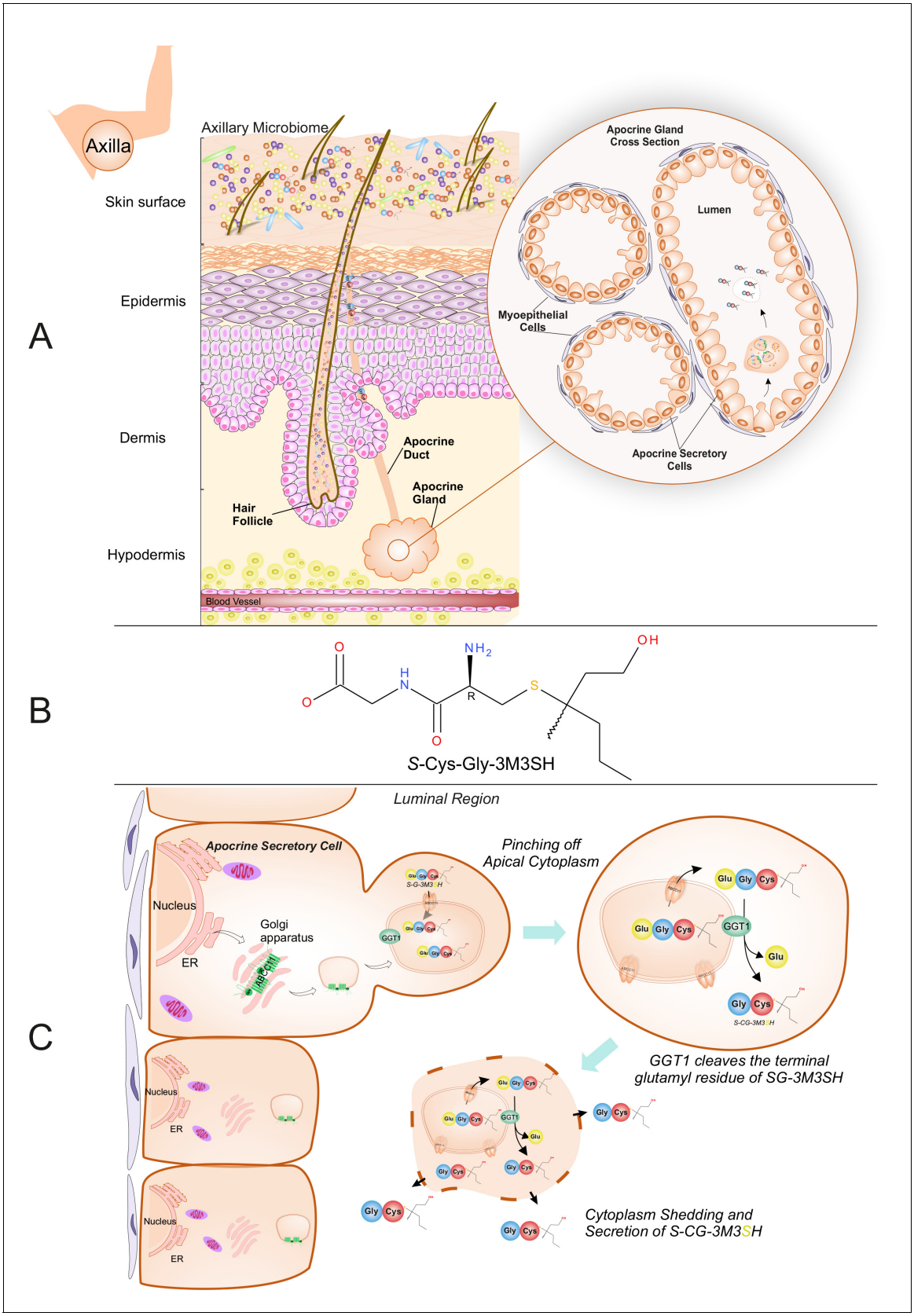

Figure 1. Biochemical route of axillary malodour precursor peptide S-Cys-Gly-3M3SH. (**A**) Schematic representation of the axilla. The surface of the skin is composed of the axillary microbiome, typically dominated by either *Corynebacterium* or Staphylococci. Axillary apocrine glands are subcutaneously

Figure 1 continued on next page

Figure 1 continued

located in the hypodermis. Apocrine glands secrete a variety of odourless precursors that are bio-transformed into odorous volatiles by the axillary microbiome. Sulfanylalkanols (e.g. 3-methyl-3-sulfanylhexan-1-ol (3M3SH)) are secreted as cysteinylglycine conjugated peptides (***Starkenmann et al., 2005***; ***Emter and Natsch, 2008***). *Staphylococcus hominis* transport and metabolise cysteinylglycine- 3-methyl-3-sulfanylhexan-1-ol (*S*-Cys-Gly-3M3SH) to liberate the odorous volatile 3M3SH, which is one of the major components of axillary malodour. (**B**) Chemical structure of the malodour precursor peptide, *S*-Cys-Gly-3M3SH. (**C**) Synthesis of *S*-Cys-Gly-3M3SH. *S*-Cys-Gly-3M3SH is derived from the glutathione 3-methyl-3-sulfanylhexanol conjugate (SG-3M3SH). SG-3M3SH is actively transported by the ATP-binding cassette transporter sub-family C member 11 (ABCC11) into apocrine secretory vesicles (***Baumann et al., 2014b***). In the secretory vesicle, *S*-Gly-3M3SH is bio-transformed by γ-glutamyl transferase 1 (GGT1), which cleaves the terminal glutamyl residue generating S-Cys-Gly-3M3SH. S-Cys-Gly-3M3SH is secreted to the surface of the skin by apocrine secretion, which characteristically involves pinching off the apical cytoplasm and partial shedding releasing intracellular components into the luminal region of the apocrine gland. Upon release the cytoplasm may be recovered and repaired and a new cycle of secretion can occur (***Farkaš, 2015***).

DOI: https://doi.org/10.7554/eLife.34995.003

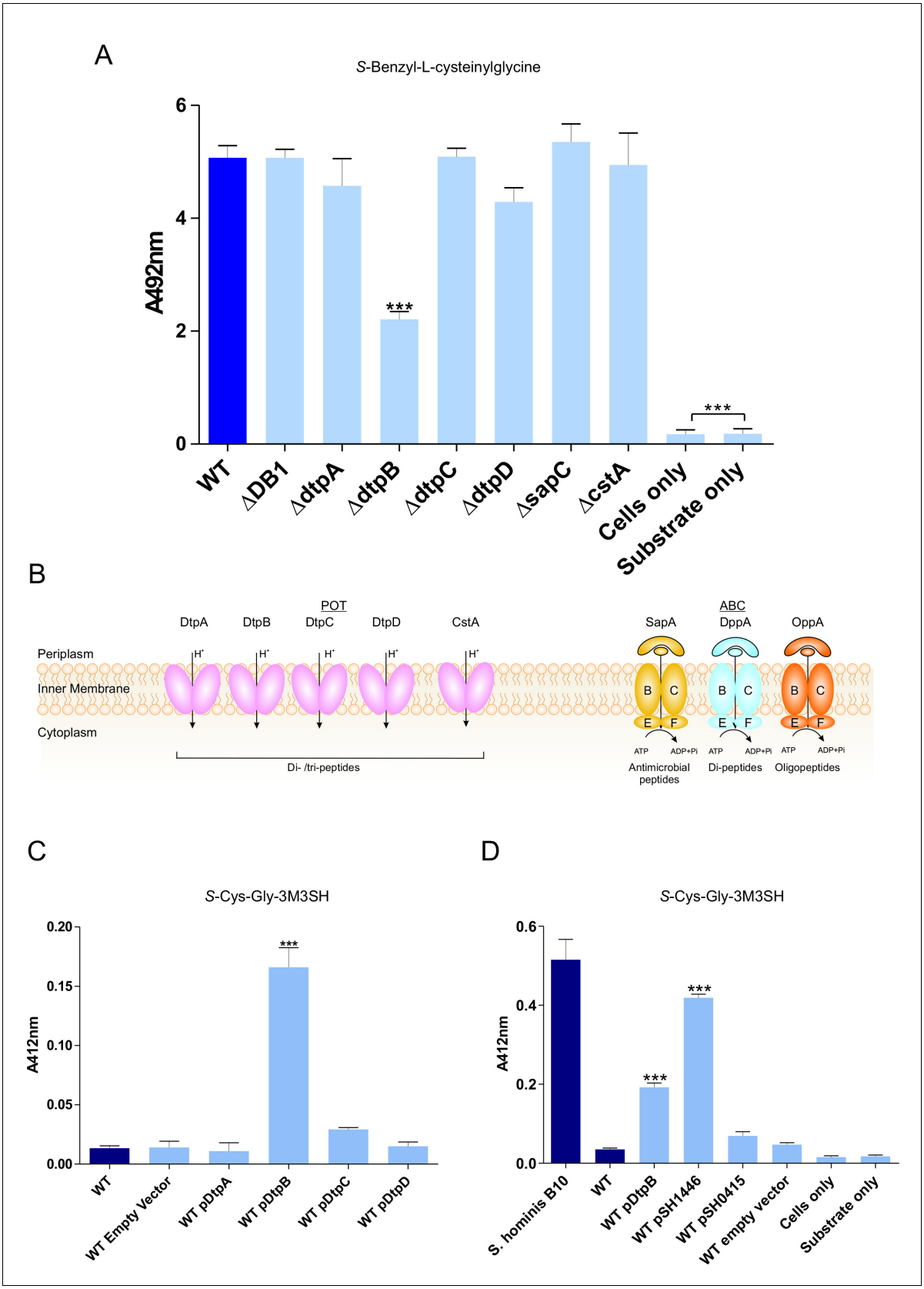

Figure 2. Biotransformation of both model (S-Benzyl-L-cysteinylglycine) and physiological substrate *S*-Cys-Gly-3M3SH by model organism *E.coli* K-12. (**A**) Biotransformation of S-Benzyl-L-cysteinylglycine by *E. coli* strains containing deletion in known or predicted peptide transporters. Strain *Δ*DB1 is an

Figure 2 continued on next page

Figure 2 continued

oppA dppA double mutant. Thioalcohol yield (A_{492}) was quantified for each strain using MTS/PMS following 4 hr incubation. (**B**) Schematic overview of the main peptide transport systems in *E. coli*. (**C**) Biotransformation of *S*-Cys-Gly-3M3SH in *E. coli* K-12 overexpressing Dtp POT transporter proteins. (**D**) *S*-Cys-Gly-3M3SH biotransformation by *E. coli* K-12 overexpressing *S. hominis* STAHO0001_1446 (pSH1446) and STAHO0001_0415 (pSH0415). *E. coli* overexpressing *dtpB* (pDtpB) is shown for reference. Thioalcohol yield (A_{412}) was quantified using DTNB after 24 hr incubation. Cultures with overexpressing plasmids were pre-induced with 0.0001% L-arabinose overnight. E. coli expressing pBADcLIC2005 with no gene insertion was included as a negative control (Empty vector). Error bars: ±SD (biological triplicates); *p<0.05, **p<0.01, ***p<0.001; One-way ANOVA followed by Dunnett's Multiple Comparison test.

DOI: https://doi.org/10.7554/eLife.34995.004

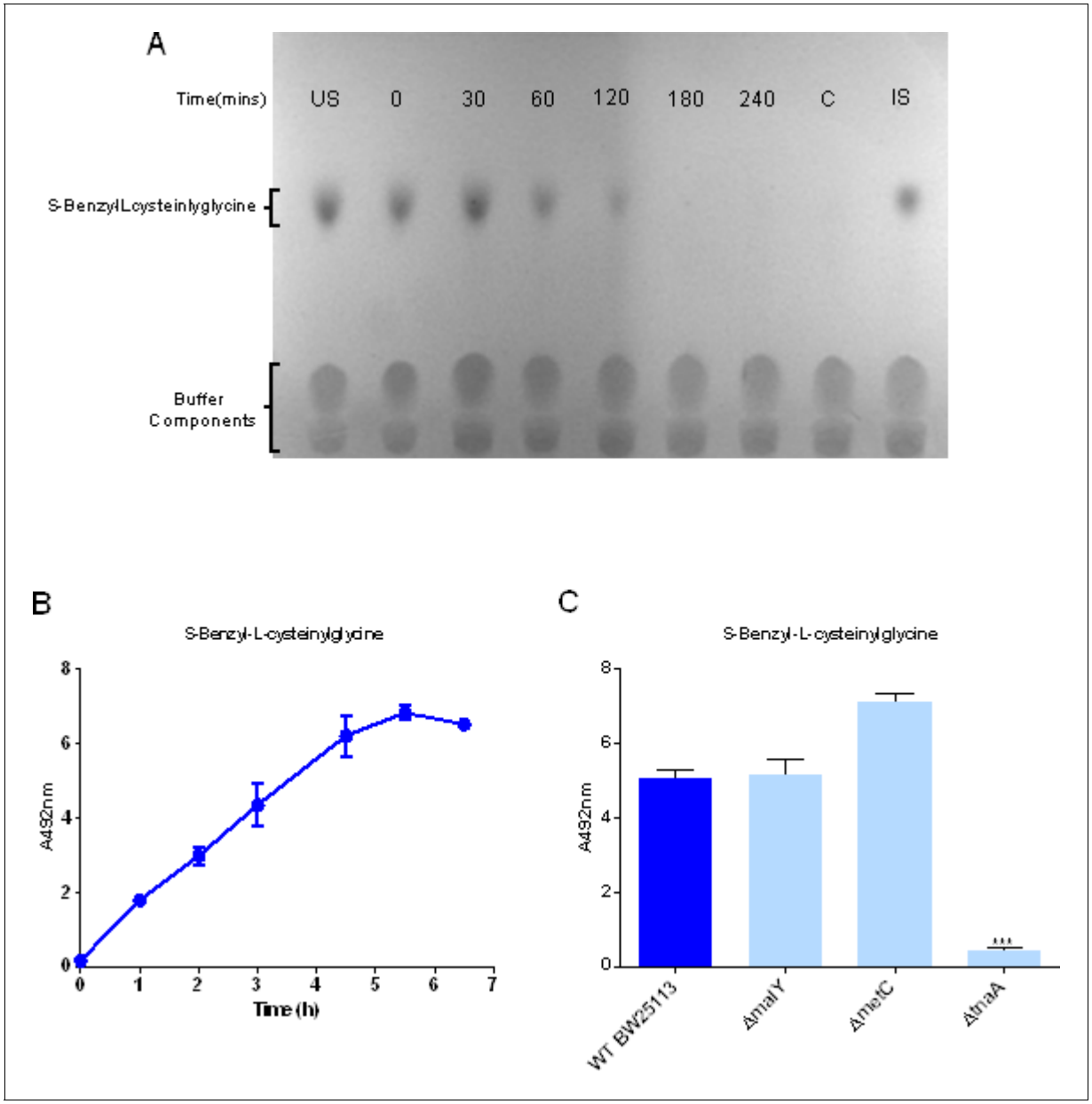

Figure 2—figure supplement 1. Uptake and biotransformation of thiol-conjugated dipeptides by *E.coli* K-12. (**A**) Thin layer chromatographic analysis of S-Benzyl-L-cysteinylglycine removal by resting *E. coli* K-12 cells at times indicated up to 240 min. The lane marked 'US' is substrate with no cells at time 0 and 'IS' is the same sample incubated at 37°C for 5 hr. The lane marked 'C' is *E. coli* cells only incubated for 5 hr in the absence of substrate. (**B**) Time dependent biotransformation of 2.5 mM S-Benzyl-L-cysteinylglycine by whole cells of *E. coli* measuring the release of benzyl mercaptan in the supernatant detected using the MTS/PMS assay and measured by the absorbance at 492 nm. Error bars represent standard deviation of three biological replicates. (**C**) S-Benzyl-L-cysteinylglycine biotransformation by *E. coli* C-S- β-lyase mutants. Thioalcohol yield (A_{492}) was quantified using MTS/PMS following 4 hr incubation. Error bars represent standard deviation of three biological replicates.

DOI: https://doi.org/10.7554/eLife.34995.005

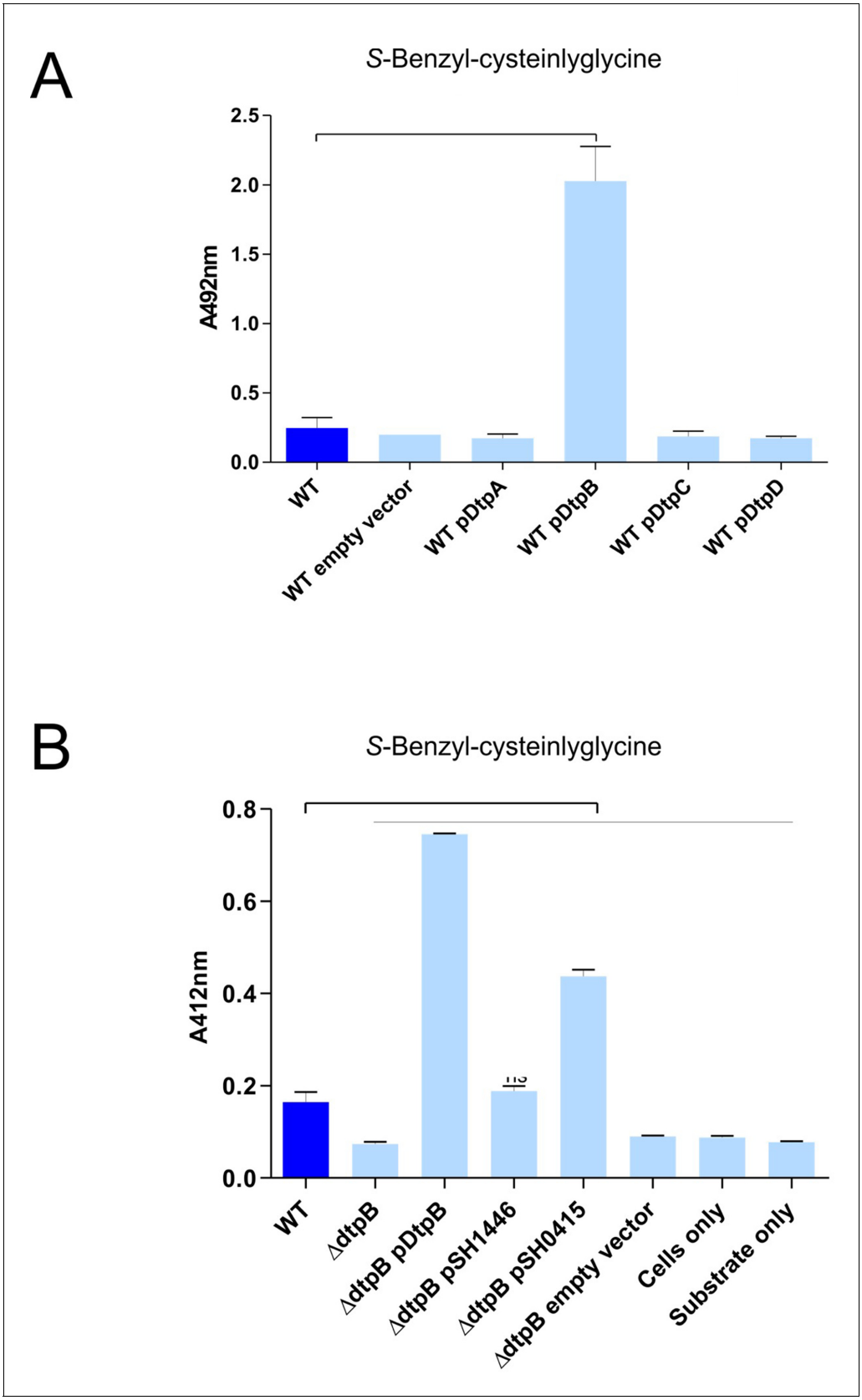

Figure 2—figure supplement 2. DtpB increases biotransformation of S-Benzyl-L-cysteinylglycine in *E. coli* K-12, while *S. hominis* transporter SH1446 does not. (**A**) Biotransformation of S-Benzyl-L-cysteinylglycine by *E. coli* K-12 overexpressing *E. coli* transporters DtpA, DtpB, DtpC, DtpD. 'Empty

Figure 2—figure supplement 2 continued on next page

Figure 2—figure supplement 2 continued

vector' refers to *E. coli* expressing pBADcLIC2005 with no gene insertion. Cultures containing strains harbouring plasmids were pre-induced with 0.0001% L-arabinose overnight. 2.5 mM S-Benzyl L-cysteinylglycine was used for all experiments. Thioalcohol yield (A_{412nm}) was quantified using DTNB after 24 hr incubation at 37˚C. Cultures with overexpressing plasmids were pre-induced with 0.0001% L-arabinose overnight. *E. coli* expressing pBADcLIC2005 with no gene insertion was included as a negative control (empty vector). Error bars: ±SD (biological triplicates). (**B**) Biotransformation of S-Benzyl-L-cysteinylglycine by *E. coli* strains, following conditions described in part (**A**), where pSH1446 and pSH0415 are the SH1446 and SH0415 genes cloned into pBADcLIC2005. Error bars: ±SD 635 (biological triplicates).

DOI: https://doi.org/10.7554/eLife.34995.006

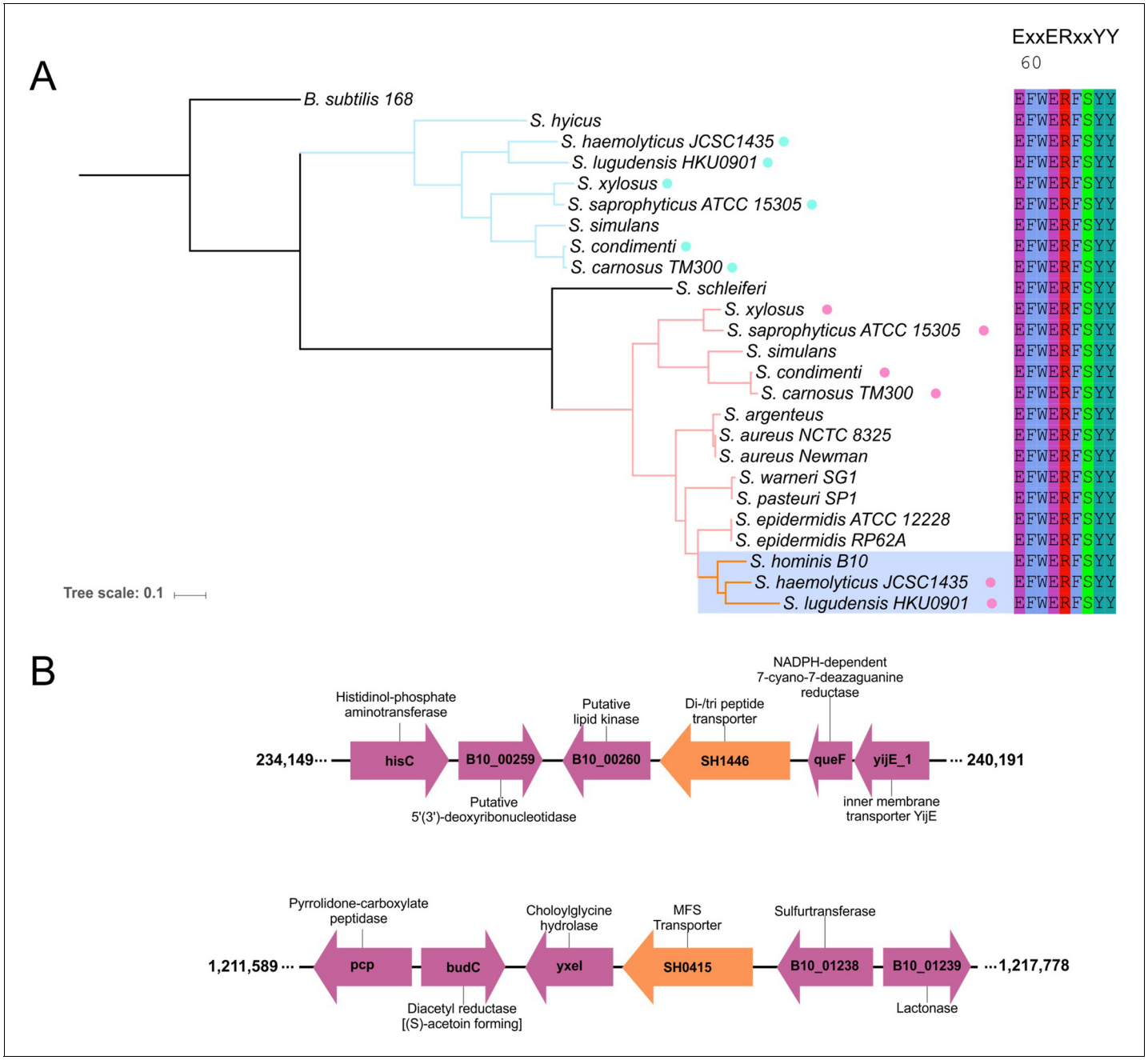

Figure 2—figure supplement 3. Phylogenetic relationship of staphylococcal SH1446 orthologues. (**A**) Genomic context of the *S. hominis* transporter genes SH1446 and SH0415 in *S. hominis* SK119. (**B**) Phylogenetic tree of staphylococci POT transporters. The tree was built using maximum likelihood with best-fit evolutionary model automatically inferred by IQ-TREE v1.5.5 (Trifinopoulos et 632 al., 2015). Blue highlighted subclade denotes malodour producing staphylococci and coloured circle represents presence of two POT's in the same species.

DOI: https://doi.org/10.7554/eLife.34995.007

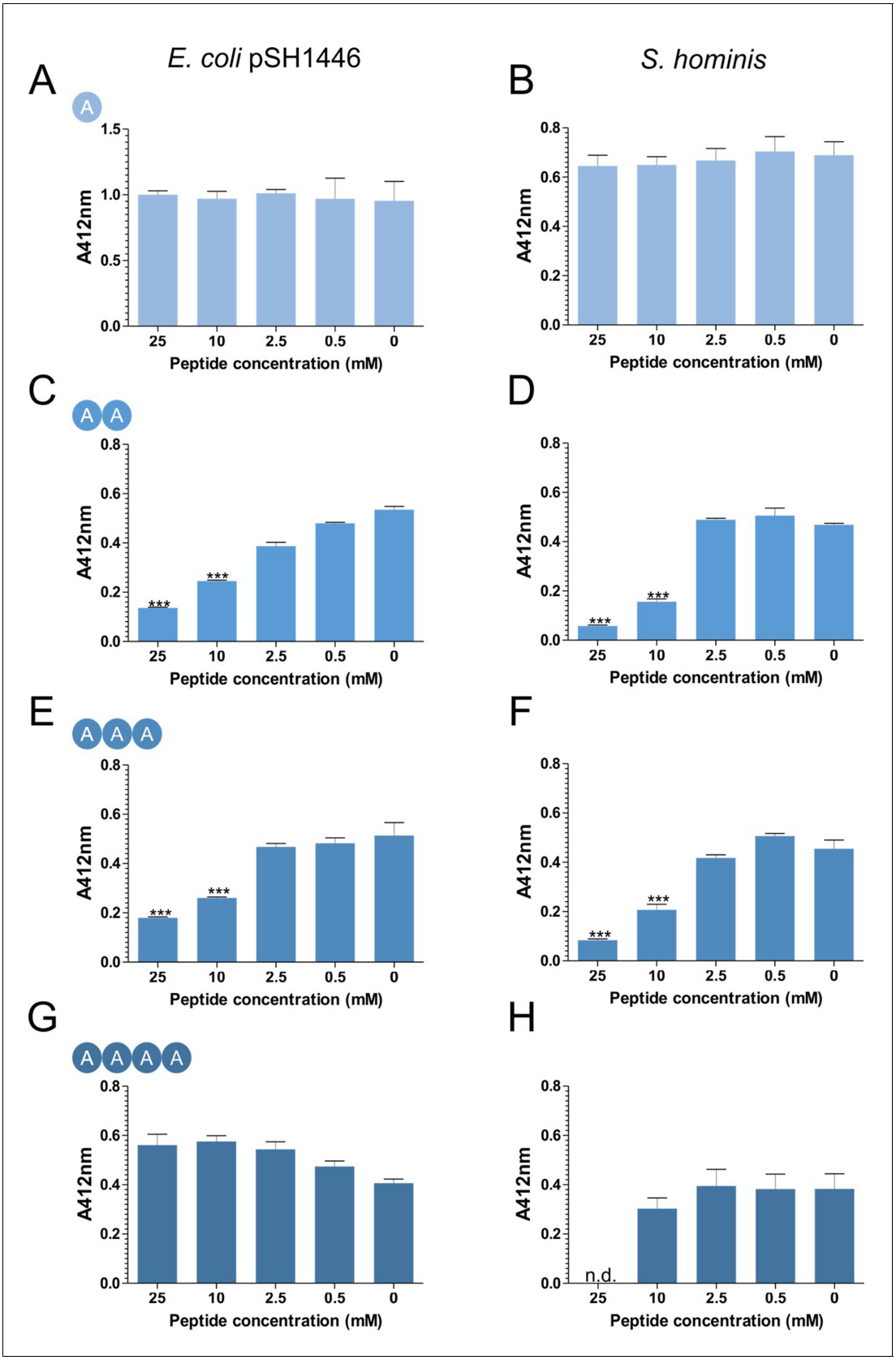

Figure 2—figure supplement 4. Inhibition of CG-3M3SH biotransformation in the presence of L-Ala peptides. Biotransformation of CG-3M3SH was determined by the DTNB assay. Cells to an OD600nm five were incubated with 2.5 mM of CG-3M3SH and various concentrations of L-Ala peptide.

Figure 2—figure supplement 4 continued on next page

Figure 2—figure supplement 4 continued

Thiolacohol yield (A412nm) was quantified after 24 hr at 37°C. *E. coli* overexpressing SH1446 was pre-induced with 0.0001% arabinose. Results are expressed as mean ± SD of biological triplicates. n.d. indicates not detected, the low pH required to dissolve tetra-Ala inhibited *S. hominis* resting cells and could not be assayed at 25 mM. Data was analysed using one-way ANOVA followed by Dunnett's Multiple Comparison test (*p<0.05, **p<0.01, ***p<0.001).

DOI: https://doi.org/10.7554/eLife.34995.008

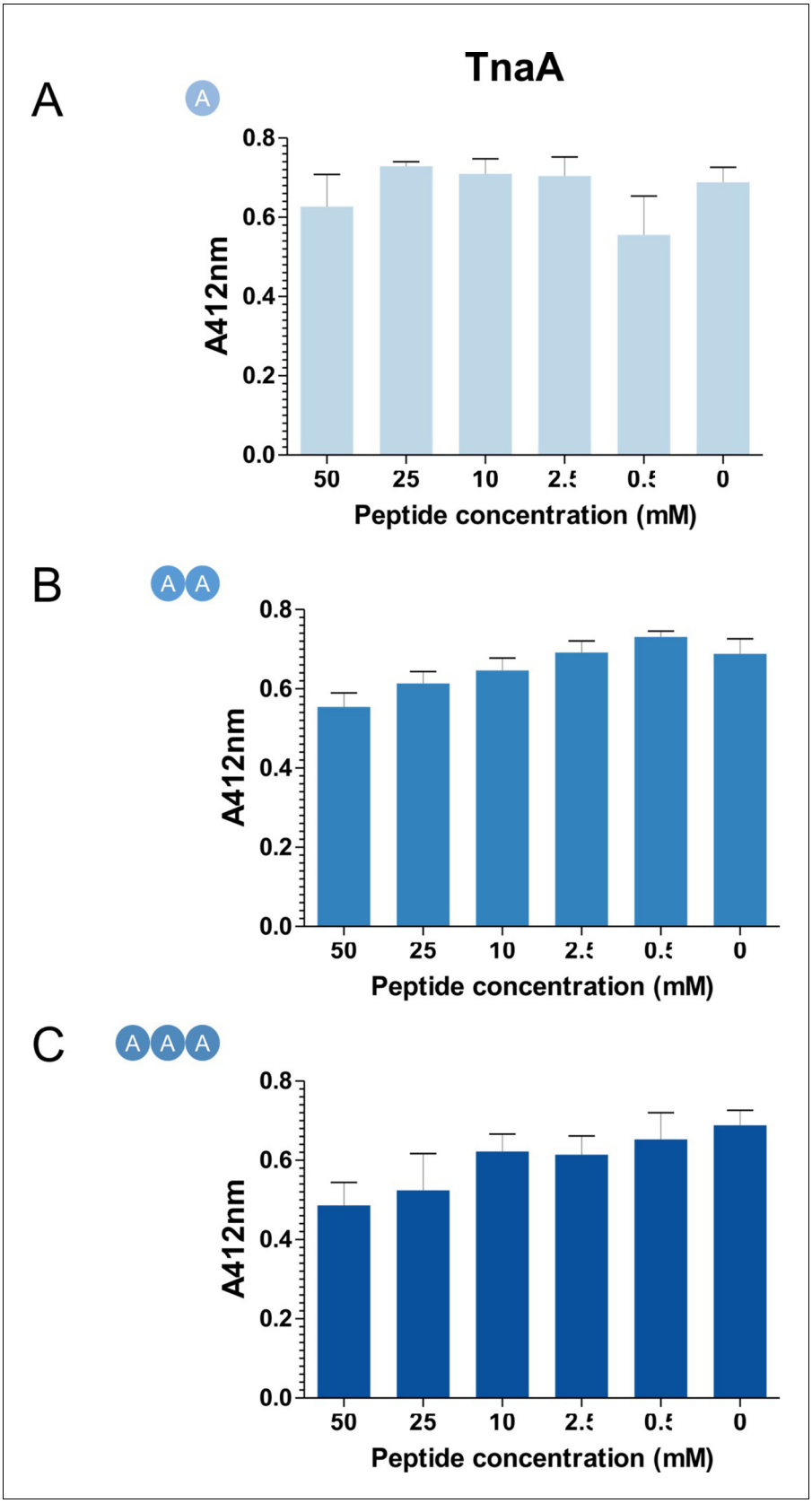

Figure 2—figure supplement 5. L-Ala peptides do not inhibit in vitro cleavage of Cys-3M3SH by TnaA. 1 µM of purified TnaA and 1 mM Cys-3M3SH substrate was incubated varying concentrations of L-Ala peptides at 37°C for 30 min. 50 µL of the reaction was labelled with DTNB and measured at

Figure 2—figure supplement 5 continued on next page

Figure 2—figure supplement 5 continued

A_{412nm}. Data are mean of biological triplicates (±SD) and was analysed using one-way ANOVA followed by Dunnett's Multiple Comparison test (*p<0.05, **p<0.01, ***p<0.001).

DOI: https://doi.org/10.7554/eLife.34995.009

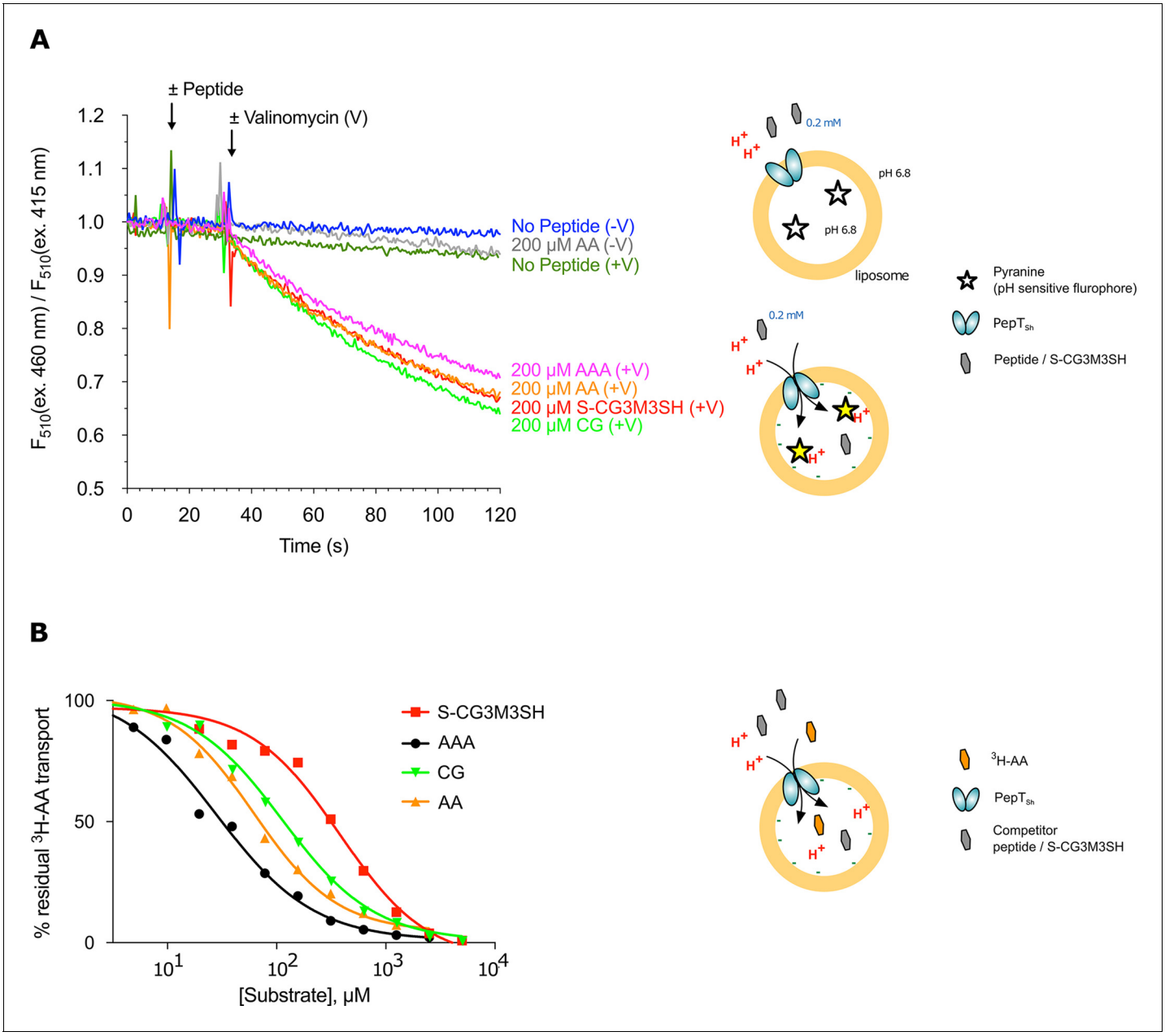

Figure 3. Functional characterisation of $PepT_{Sh}$. (**A**) Monitoring proton coupled peptide uptake using a pH sensitive dye. $PepT_{Sh}$ was reconstituted into liposomes loaded with pyranine and a high concentration of potassium ions. The external solution contains either peptide, Ala-Ala (orange), Ala-Ala-Ala (purple), Cys-Gly (Green) or S-Cys-Gly-3M3SH (red) and a low potassium concentration. On addition of valinomycin (V) the membrane becomes highly permeable to potassium, generating a hyperpolarised membrane potential (negative inside), which drives the uptake of protons and ligand, protonating the pyranine dye and altering its fluorescent properties. A change in the ratio of fluorescence demonstrates active transport of the ligand. (**B**) Representative IC_{50} curves showing the relative affinity of the different ligands shown in A for $PepT_{Sh}$. Assays were set up to measure the ability of competitor peptides to reduce uptake of tritiated di-Alanine (AA) peptide.

DOI: https://doi.org/10.7554/eLife.34995.010

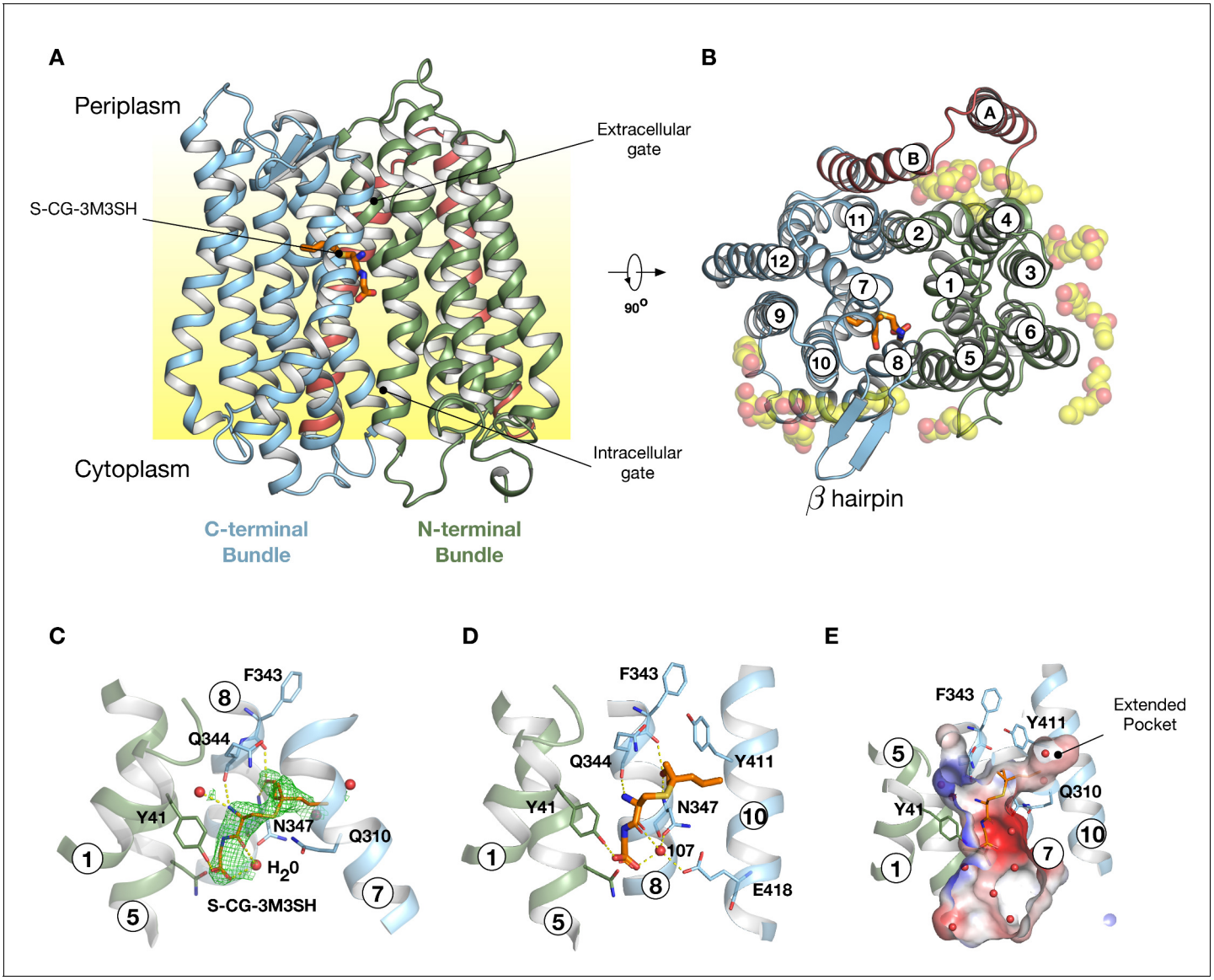

Figure 4. Crystal structure of $PepT_{Sh}$. (**A**) Crystal structure of $PepT_{Sh}$ shown in the plane of the membrane. Transmembrane helices making up the N-terminal bundle, H1-H6, are coloured green and pack against the C-terminal bundle, helices H7-H12. The bound S-Cys-Gly-3M3SH peptide is shown in sticks. (**B**) View of A rotated 90 °. The additional helices, HA and HB, can be clearly observed packing to one side of the transporter. The bound lipids are shown as spheres. (**C**) Zoomed in view of the binding site showing the bound S-Cys-Gly-3M3SH ligand with the mFo-DFc difference electron density map contoured at 3 σ in green mesh. (**D**) Equivalent view of the binding site showing the location of ordered water molecules in the binding site. (**E**) View showing the electrostatic surface of the binding site of the transporter with the hydrophobic pocket accommodating the acyl chain of the ligand.
DOI: https://doi.org/10.7554/eLife.34995.011

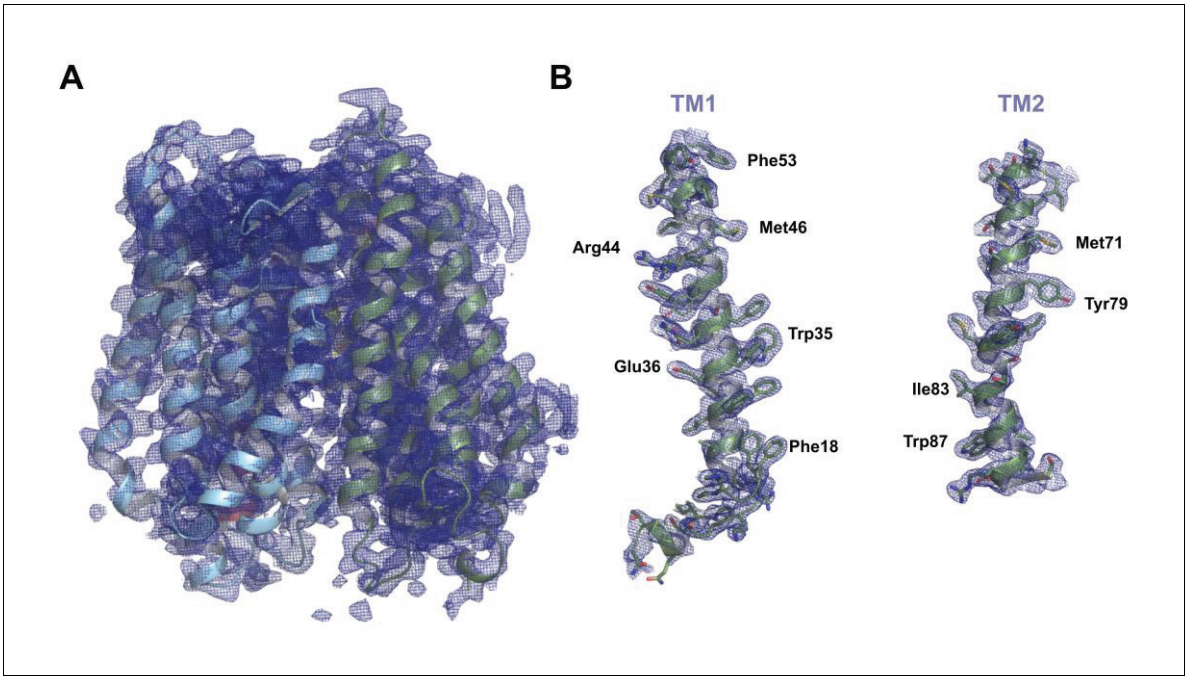

Figure 4—figure supplement 1. Final refined electron density map for $PepT_{Sh}$. (**A**) Final refined 2m*Fo*-D*Fc* electron density map for $PepT_{Sh}$, contoured at 1σ. (**B**) Zoomed in view of the electron density map for H1 and H2, with specific side chains labelled.

DOI: https://doi.org/10.7554/eLife.34995.012

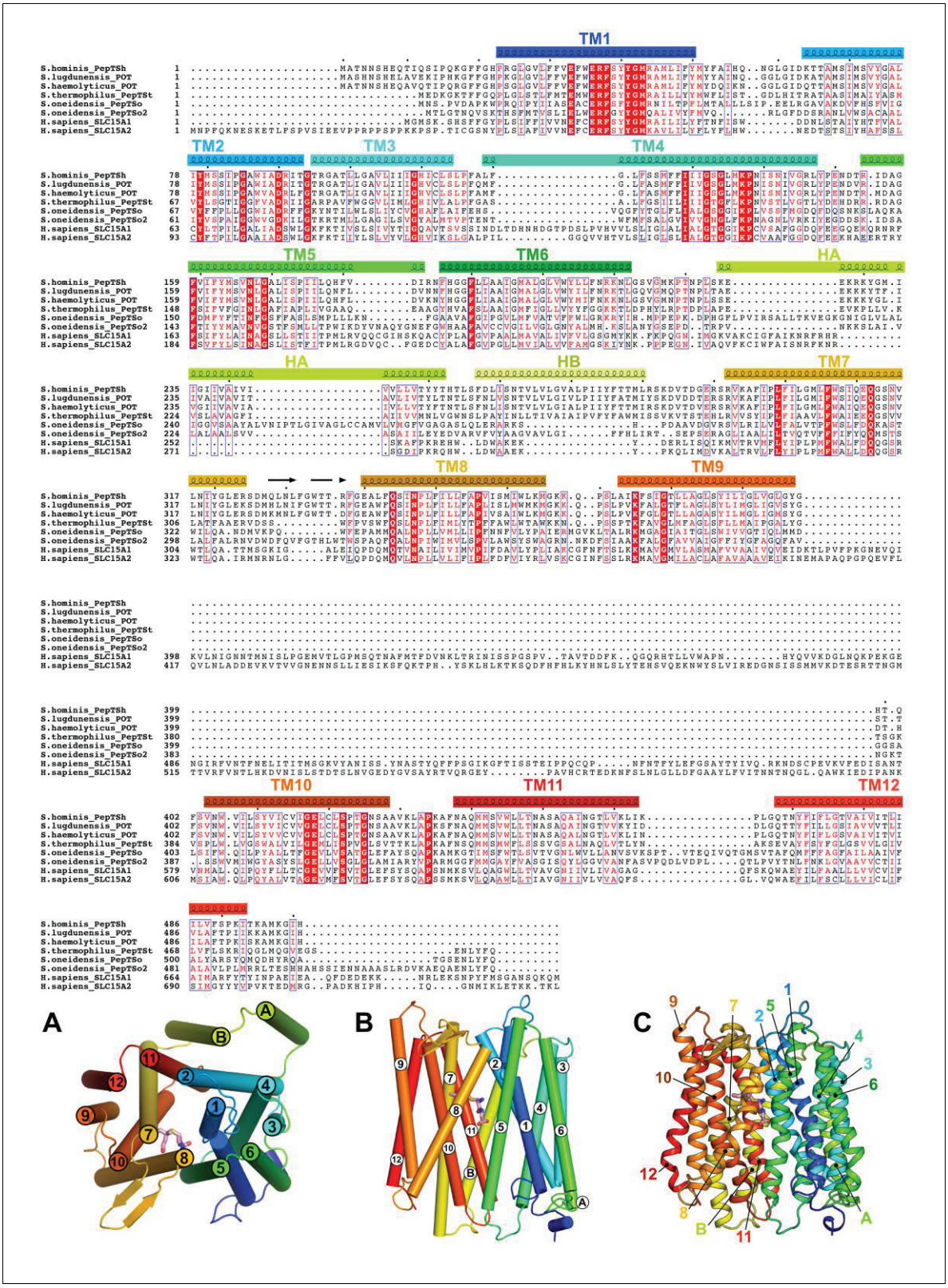

Figure 4—figure supplement 2. Sequence alignment of $PepT_{Sh}$ with bacterial species found in the human axilla and human peptide transporters. Strictly conserved amino acids are shown in red. Similar amino acids are enclosed in blue boxes. The position of Transmembrane helices from $PepT_{Sh}$ are highlighted above the protein sequence and coloured according to the structure at the bottom: (**A**) perspective of the peptide transporter looking down, from the extracellular side of the membrane, (**B**) cylindrical representation of the transmembrane helices, as viewed from the plane of the

Figure 4—figure supplement 2 continued on next page

Figure 4—figure supplement 2 continued

membrane, and in the same orientation (**C**), with cartoon representation of the helices. The conserved motif on helix H10 is highlighted by the dashed black box.

DOI: https://doi.org/10.7554/eLife.34995.013

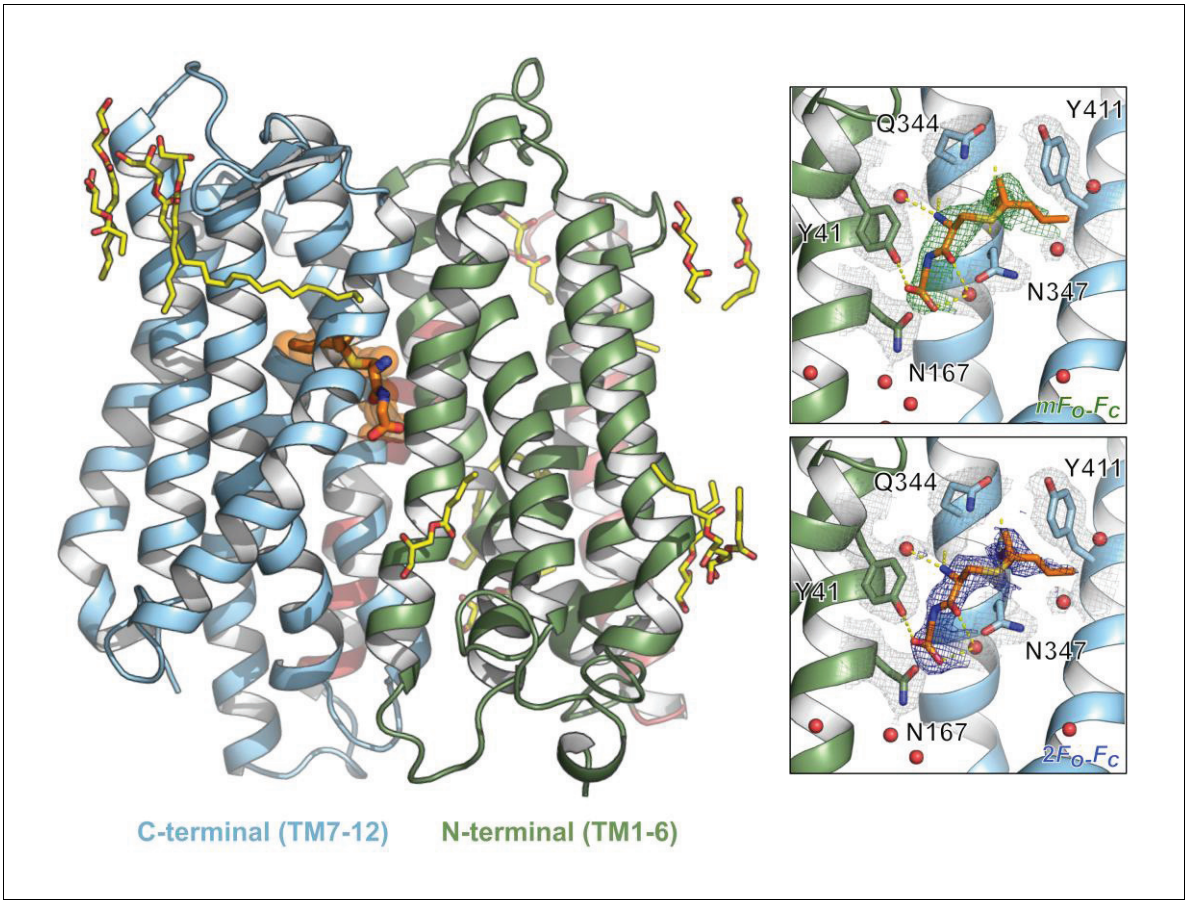

Figure 4—figure supplement 3. Structure of $PepT_{Sh}$ bound to the modified peptide S-Cys-Gly-3M3SH. Cartoon representation of $PepT_{Sh}$ viewed from the plane of the membrane. The N- and C-terminal bundles are coloured green and blue respectively. S-Cys-Gly-3M3SH is modelled as orange sticks against a background of transparent orange spheres showing the molecular volume. Monoolein lipids of varying lengths, as observed by their electron density, are displayed as yellow sticks. **Inset:** S-Cys-Gly-3M3SH was modelled into experimental difference density (green, mFo–DFc contoured at 3σ) and the final refined density is shown in blue (2mFo–DFc, contoured at 1σ). Key residues in close proximity of S-Cys-Gly-3M3SH are highlighted with their electron density shown in grey, contoured at 1σ. Nearby water molecules were modelled as red spheres.

DOI: https://doi.org/10.7554/eLife.34995.014

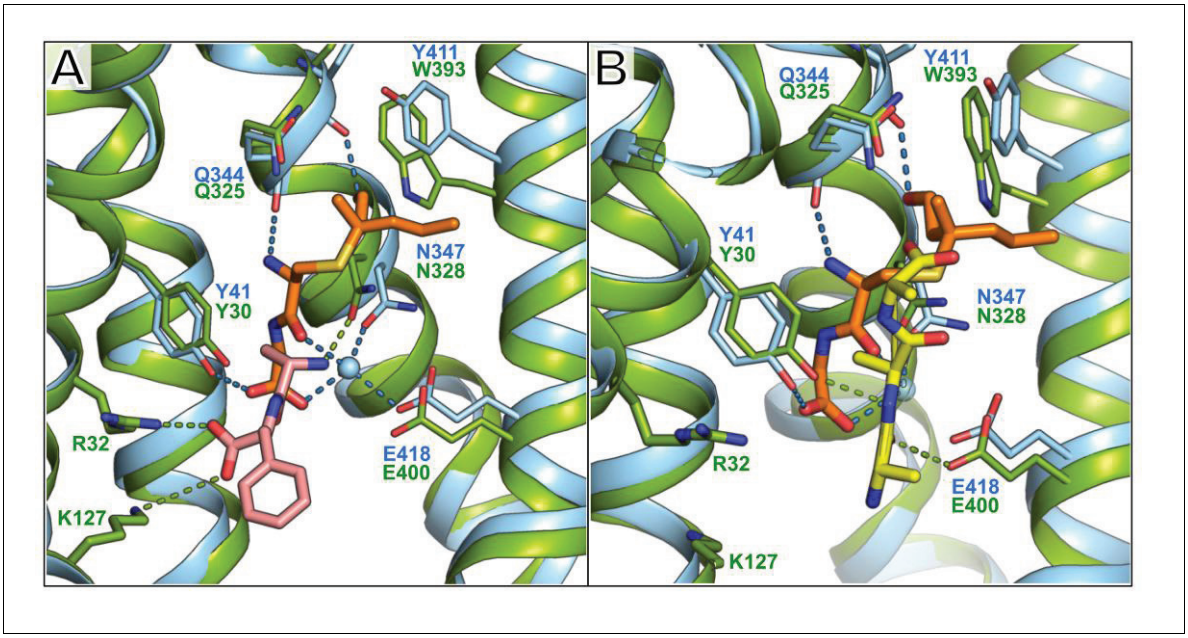

Figure 4—figure supplement 4. Comparison between the binding position of S-Cys-Gly-3M3SH and the natural di- and tri-peptides co-crystallised with $PepT_{St}$. (**A**) $PepT_{Sh}$ (blue) bound with S-Cys-Gly-3M3SH (orange) overlaid with $PepT_{St}$ (green) bound with L-Ala-L-Phe (pink sticks) (PDB: 4D2C). (**B**) Equivalent view of $PepT_{Sh}$ in (**A**) but overlaid with the tri-Ala (yellow sticks) co-crystal structure of $PepT_{St}$ (PDB: 4D2D). The dipeptide moiety of interacts with the conserved E^{33}xxERxYY^{41} motif with further interactions through the highly conserved Asn347. Backbone mediated interactions from Gln344 and Phe343 help stabilise the substrate in a vertical orientation.

DOI: https://doi.org/10.7554/eLife.34995.015

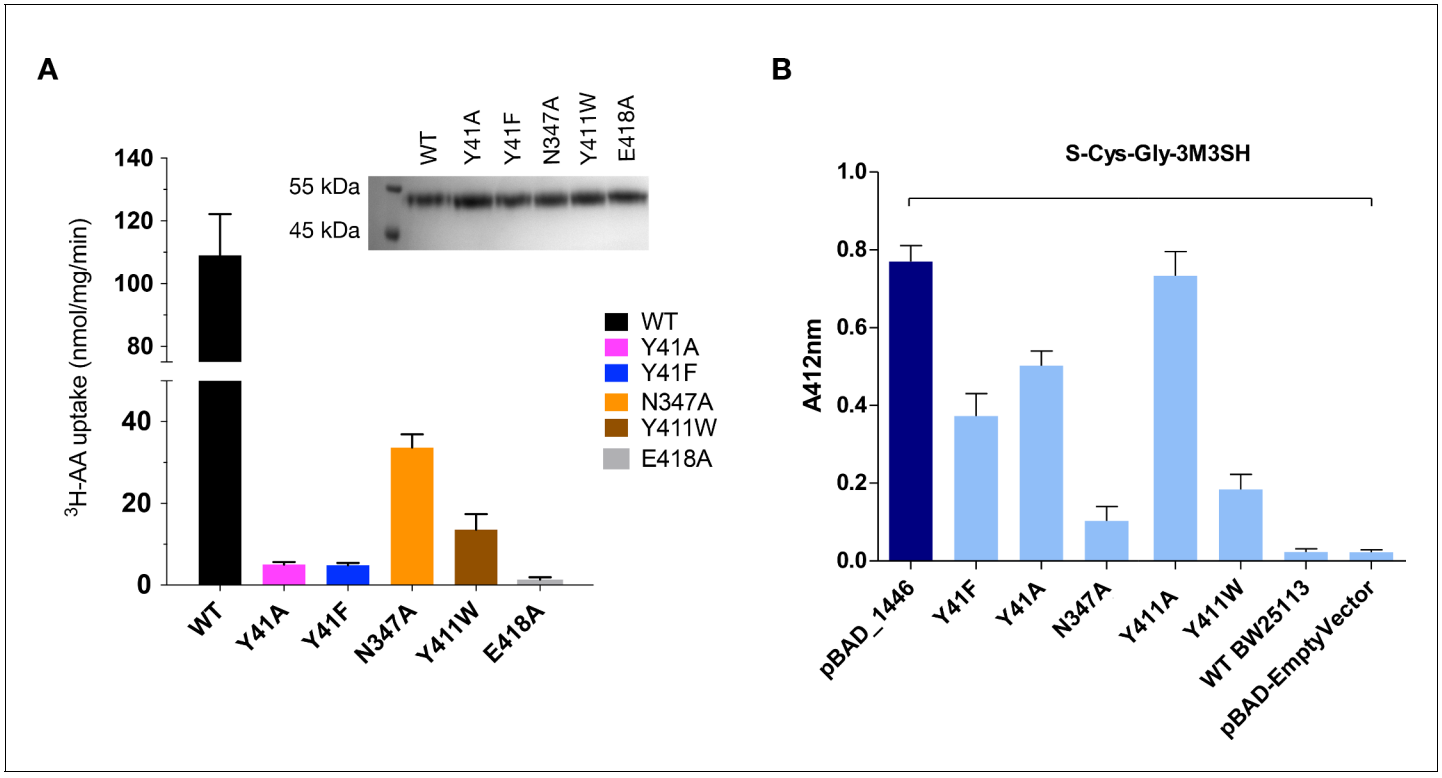

Figure 5. Functional characterisation of binding site residues. (**A**) Bar chart showing the di-alanine uptake for the WT and mutant variants of $PepT_{Sh}$. Inset – SDS-PAGE analysis of the reconstituted proteins used in the assay. (**B**) Biotransformation of *S*-Cys-Gly-3M3SH by *E. coli* K-12 (BW25113) overexpressing WT $PepT_{St}$ (pBAD_1446), or variants indicated, compared to background uptake in non-transformed cells (WT BW25113) and cells harbouring empty plasmid (pBAD-EmptyVector). Error bars: ±SD (biological triplicates).

DOI: https://doi.org/10.7554/eLife.34995.017

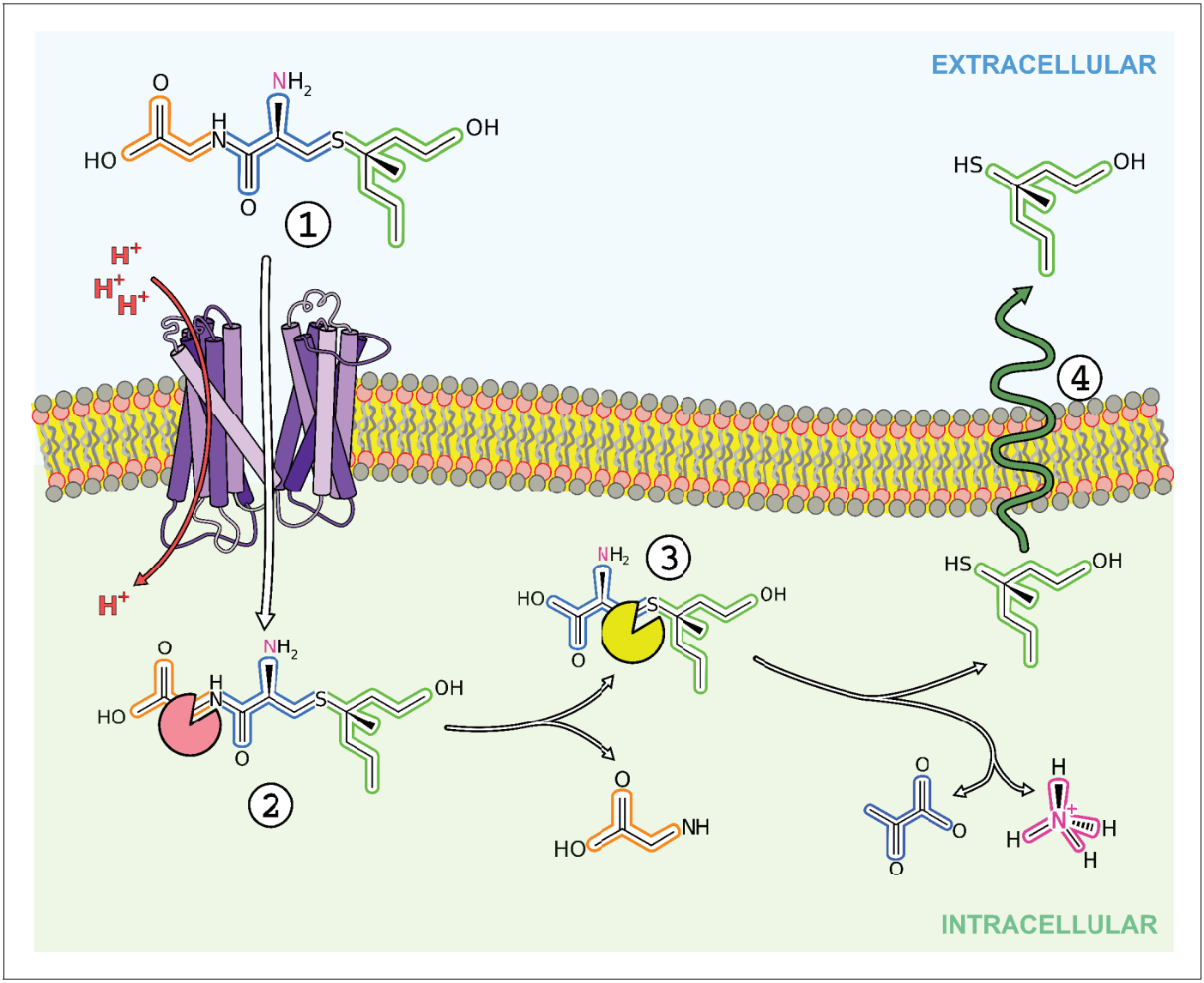

Figure 6. Overview of transport and intracellular biotransformation of *S*-Cys-Gly-3M3SH in *Staphylococcus hominis*. 1. Cys-Gly-(*S*)−3M3SH is actively transported across the membrane by the di/tri peptide transporter $PepT_{Sh}$ along with the movement of protons. 2. A dipeptidase cleaves the terminal glycine residue of *S*-Cys-Gly-3M3SH producing Cys-(*S*)−3M3SH. 3. The thiol is liberated from Cys-(S)−3M3SH by a C-S β-lyase that also releases ammonia and pyruvate, the volatile thiol (3M3SH) then diffuses or is exported out the cell. 4.

DOI: https://doi.org/10.7554/eLife.34995.018